Oncogenic β-catenin triggers an inflammatory response that determines the aggressiveness of hepatocellular carcinoma in mice

Marie Anson,[1,2,3,4] Anne-Marie Crain-Denoyelle,[1,2,3,4] Véronique Baud,[1,2,3] Fanny Chereau,[1,2,3] Angélique Gougelet,[1,2,3] Benoit Terris,[1,2,3,5] Satoshi Yamagoe,[6] Sabine Colnot,[1,2,3] Mireille Viguier,[1,2,3,4,7] Christine Perret,[1,2,3] and Jean-Pierre Couty[1,2,3,4]

[1]INSERM, U1016, Institut Cochin, Paris, France. [2]CNRS, UMR8104, Paris, France. [3]Université Paris Descartes, Sorbonne Paris Cité, Paris, France. [4]Université Paris Diderot, Sorbonne Paris Cité, Paris, France. [5]GHU Ouest, Groupe Hospitalier Cochin, Saint-Vincent de Paul, Hôpital Cochin, AP-HP, Service d'anatomie et de Cytologie Pathologiques, Paris, France. [6]Department of Bioactive Molecules, National Institute of Infectious Diseases, Shinjuku-ku, Tokyo, Japan. [7]Institut Jacques Monod, Université Paris-Diderot, CNRS UMR 7592, Paris, France.

Hepatocellular carcinoma (HCC) is the third leading cause of cancer-related death worldwide. Its pathogenesis is frequently linked to liver inflammation. Gain-of-function mutations in the gene encoding β-catenin are frequent genetic modifications found in human HCCs. Thus, we investigated whether inflammation was a component of β-catenin–induced tumorigenesis using genetically modified mouse models that recapitulated the stages of initiation and progression of this tumoral process. Oncogenic β-catenin signaling was found to induce an inflammatory program in hepatocytes that involved direct transcriptional control by β-catenin and activation of the NF-κB pathway. This led to a specific inflammatory response, the intensity of which determined the degree of tumor aggressiveness. The chemokine-like chemotactic factor leukocyte cell–derived chemotaxin 2 (LECT2) and invariant NKT (iNKT) cells were identified as key interconnected effectors of liver β-catenin–induced inflammation. In genetic deletion models lacking the gene encoding LECT2 or iNKT cells, hepatic β-catenin signaling triggered the formation of highly malignant HCCs with lung metastasis. Thus, our results identify inflammation as a key player in β-catenin–induced liver tumorigenesis. We provide strong evidence that, by activating pro- and antiinflammatory mediators, β-catenin signaling produces an inflammatory microenvironment that has an impact on tumoral development. Our data are consistent with the fact that most β-catenin–activated HCCs are of better prognosis.

Introduction

Cumulative evidence indicates that chronic inflammatory diseases result in a predisposition to various types of cancers (1, 2). An inflammatory component is present in the microenvironment of most neoplastic tissues, including those that are not causally related to an obvious inflammatory process (2). Recent data have shown that different genetic alterations occurring in tumor cells activate an inflammatory program that has a profound impact on cancer development (3). Oncogenic transcription factors such as NF-κB and STAT3, together with inflammatory cytokines, have been defined as key orchestrators of the intricate dialogue among the components of the immune system present in the tumor microenvironment and cancerous cells (3, 4).

Hepatocellular carcinoma (HCC) is the third leading cause of cancer-related death worldwide. It develops frequently within the context of chronic hepatitis, which is characterized by liver inflammation and hepatocyte apoptosis (5). Interestingly, the adult liver contains a specific microenvironment composed of immune cells dedicated to preventing the chronic inflammation that could potentially result from the liver parenchyma's constant exposure to the dietary and environmental carcinogens present in the blood arriving from the gut (6). Because chronic liver inflammation and the associated regenerative wound-healing responses are strongly linked to the development of HCC, it is not surprising that the liver's inflammatory response is tightly regulated. In addition, inflammation seems to be a key promoter that drives maladaptive wound-healing responses (7).

One of the major pathways involved in hepatocellular carcinogenesis is the Wnt/β-catenin pathway (8, 9). Aberrant β-catenin signaling, mainly due to mutations in the β-catenin gene, is found in 30%–40% of human HCCs (9, 10). Mutant β-catenins translocate into the nucleus and activate a Wnt/β-catenin–dependent gene transcription program that promotes tumorigenesis. However, the mechanisms by which aberrant Wnt/β-catenin pathway activation leads to the development of HCC are not completely understood. Several molecular integrative studies have revealed that β-catenin–mutated HCCs exhibit specific morphological and metabolic features associated with more favorable prognoses and can be grouped within a homogeneous HCC subclass (11–13). This suggests that β-catenin–activated HCCs develop via a common carcinogenic pathway.

We decided to investigate whether inflammation was a component in the process of β-catenin–induced liver tumorigenesis. Using genetic models that recapitulated different stages of β-catenin–induced hepatocellular transformation, we demonstrated that β-catenin signaling induces an inflammatory program in hepatocytes that involves direct transcriptional control by β-catenin and activation of the NF-κB pathway. This leads to a specific inflammatory response, the intensity of which determines the

Authorship note: Mireille Viguier and Christine Perret contributed equally to this work.

Conflict of interest: The authors have declared that no conflict of interest exists.

Citation for this article: *J Clin Invest.* 2012;122(2):586–599. doi:10.1172/JCI43937.

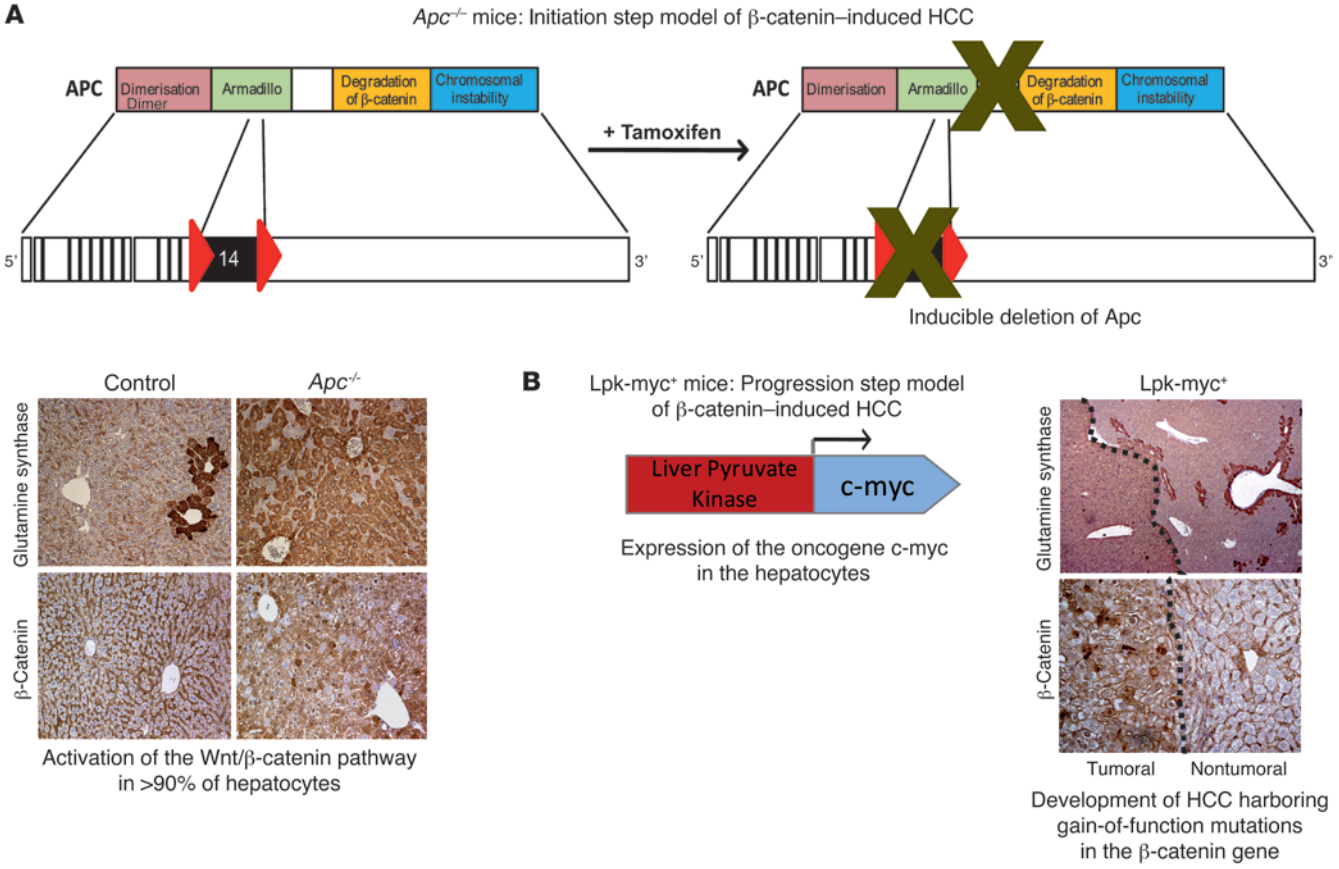

Figure 1
Description of the different genetically modified mouse models harboring oncogenic β-catenin activation in the liver. (**A**) Initiation step model of β-catenin–induced HCC. In this previously described model (14, 15), *Apc* inactivation in nearly all hepatocytes of the liver lobule is induced by tamoxifen injection and is evidenced by glutamine synthetase, cytosolic, and nuclear β-catenin stainings. $Apc^{flox/flox}$, TTR-Cre-Tam mice are referred to as $Apc^{-/-}$ mice and $Apc^{flox/flox}$, Cre-negative mice are control mice. (**B**) Progression step model of β-catenin–induced HCC. In this previously described model (9, 16), expression of the c-myc oncogene is targeted in the hepatocytes under the control of the *Lpk* gene and leads to the development of HCCs that harbor activated β-catenin mutations (9, 16) and stain positive for glutamine synthetase and nuclear β-catenin.

degree of tumor aggressiveness. We identified 2 interconnected key mediators of liver β-catenin–induced inflammatory response: the chemokine-like chemotactic factor leukocyte cell–derived chemotaxin 2 (LECT2), and invariant NKT cells (iNKT). In genetic deletion models lacking the *LECT2* gene or iNKT cells, β-catenin signaling triggered the development of highly malignant HCCs that also metastasized to the lung. Our results identify, for what we believe is the first time, inflammation as a key player in β-catenin–induced liver tumorigenesis and provide strong evidence that, by activating pro- and antiinflammatory mediators, β-catenin signaling produces an inflammatory milieu that determines the aggressiveness of the tumor.

Results

To study the role of the liver microenvironment during β-catenin–induced tumorigenesis, we took advantage of 2 different genetic mouse models that we previously described as mimicking 2 of the steps (initiation and progression) involved in the tumoral process induced by oncogenic activation of β-catenin signaling in hepatocytes (Figure 1A). The first model reproduces the initial step of β-catenin oncogenesis and is based on the tamoxifen-inducible hepatospecific inactivation of the tumor suppressor gene adenomatous polyposis coli ($Apc^{-/-}$). All hepatocytes of the liver lobule show aberrant activation of β-catenin after tamoxifen injection (14, 15). Because $Apc^{-/-}$ animals die at an early age (15), we used the transgenic Lpk-myc$^+$ mouse model to study tumor progression, since these mice developed HCC-bearing activating mutations in the β-catenin gene (Figure 1B and refs. 9, 16). Indeed, in contrast with the intestine, in which c-myc oncogene is a critical target of the Wnt signaling pathway that drives tumorigenesis, we demonstrated, using a combination of several molecular approaches (ChIP-seq, RNA-Seq), that c-myc was not a target of Wnt signaling in the liver (15, 17–19). In this model, c-myc and β-catenin signaling cooperate to drive liver carcinogenesis.

β-catenin activation in hepatocytes modifies the liver microenvironment and results in specific targeting of iNKT cells. To evaluate the impact of hepatocyte β-catenin activation on the liver microenvironment at an early step of hepatocarcinogenesis, we purified and analyzed nonparenchymal cells (NPCs) from $Apc^{-/-}$ mouse livers 5 and 8 days after tamoxifen injection and compared them with the NPCs of control mice. In agreement with our previous findings (14),

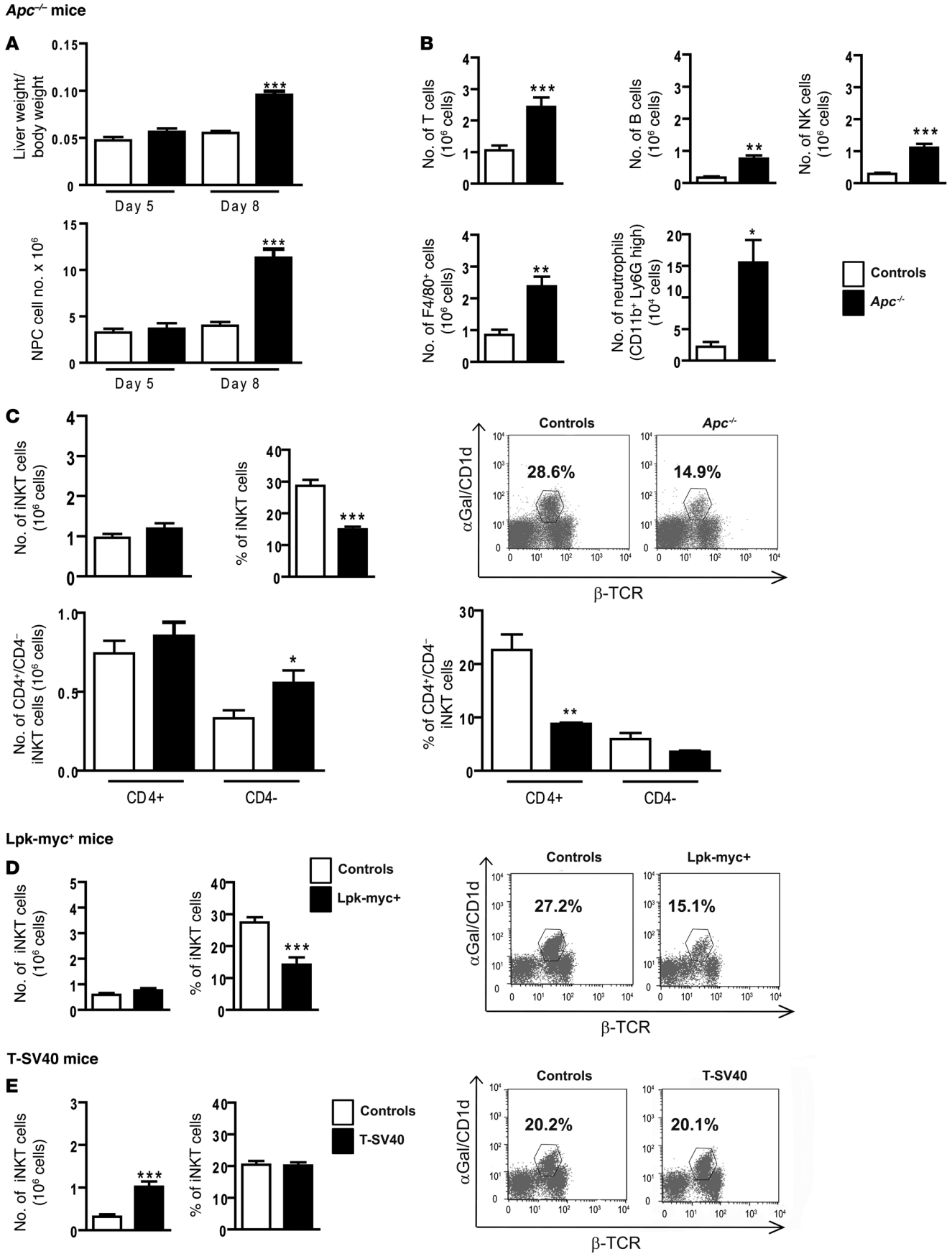
Apc-/- mice
A
Liver weight/ body weight
Day 5
Day 8
NPC cell no. x 10^6
B
No. of T cells (10^6 cells)
No. of B cells (10^6 cells)
No. of NK cells (10^6 cells)
No. of F4/80+ cells (10^6 cells)
No. of neutrophils (CD11b+ Ly6G high) (10^4 cells)
Controls
Apc-/-
C
No. of iNKT cells (10^6 cells)
% of iNKT cells
Controls
Apc-/-
28.6%
14.9%
αGal/CD1d
β-TCR
No. of CD4+/CD4- iNKT cells (10^6 cells)
% of CD4+/CD4- iNKT cells
CD4+
CD4-
Lpk-myc+ mice
D
Controls
Lpk-myc+
27.2%
15.1%
T-SV40 mice
E
Controls
T-SV40
20.2%
20.1%

Figure 2
β-catenin activation in hepatocytes modifies the liver microenvironment and specifically affects iNKT cell recruitment. (**A**) The ratio of liver weight/body weight was assessed, and the number of NPCs was evaluated in control and *Apc*$^{-/-}$ livers at 5 and 8 days after tamoxifen injection. (**B**) FACS analysis of NPCs was performed to assess the absolute number (Nb) of the various immune cell subpopulations (T cells, B cells, F4/80-positive cells, neutrophils, and NK cells) in *Apc*$^{-/-}$ and control livers, 8 days after tamoxifen injection. (**C**) FACS analysis of NPCs from *Apc*$^{-/-}$ and control livers was performed using α-GalCer/CD1d tetramer expression to assess the number (upper left panel) and proportion (upper right panel) of iNKT cells in the total population and the number (lower left panel) and proportion (lower right panel) of iNKTs expressing or not expressing the CD4 marker. (**D**) FACS analysis of NPCs was performed using α-GalCer/CD1d tetramer expression to assess the number (left panel) and the proportion (right panel) of iNKT cells in 12-month-old tumoral Lpk-myc^{+} livers and nontumoral control livers. (**E**) FACS analysis of NPCs was performed using α-GalCer/CD1d tetramer expression to assess the number (left panel) and the proportion (right panel) of iNKT cells in T-SV40 and control livers. The graphs represent the number or the proportion of cells among CD45^{+}/Ly5^{+} cells in the liver. Dot plots show representative FACS analysis, and the numbers represent the percentage of iNKTs gated on CD45^{+}Ly5^{+} cells. All data are representative of 6 independent experiments with 4 mice/group. $^{*}P < 0.05$; $^{**}P < 0.01$; $^{***}P < 0.001$ (controls vs. *Apc*$^{-/-}$ or controls vs. Lpk-myc^{+} or controls vs. T-SV40). Error bars represent SD.

mice injected with tamoxifen developed progressive hepatomegaly (Figure 2A) that was simultaneously associated with significantly higher total numbers of NPCs (Figure 2A). Results from cell cycle analysis strongly suggested that most NPCs found in the liver of *Apc*$^{-/-}$ mice were recruited from outside the liver and contained a modest fraction of in situ proliferating cells (Supplemental Figure 1A; supplemental material available online with this article; doi:10.1172/JCI43937DS1). We then used FACS to characterize the different populations of immune cells present in the liver of animals following hepatocyte β-catenin activation and in the livers of control animals. We detected higher absolute numbers of most types of immune cells in the livers of tamoxifen-treated mice, including Kupffer cells (F4/80 positive), granulocytes (Gr1 positive cells), NK, B lymphocytes, and conventional T cells (Figure 2B). However, for all these immune populations, their respective proportions among the total infiltrating immune cells (CD45^{+} cells) remained unchanged (Supplemental Figure 1B).

Remarkably, we found that the iNKT population responded differently; their absolute numbers in *Apc*$^{-/-}$ livers were not higher relative to those in control livers. This resulted therefore in a dramatic proportional decrease of iNKT cells in the entire population of immune cells (*Apc*$^{-/-}$, 14.9%, versus controls, 28.6%) (Figure 2C). These cells are called iNKTs due to their nonpolymorphic TCR, which exclusively recognizes the α-galactosylceramide (α-GalCer) lipid as an antigen presented by MHC class I–like CD1d molecules (20). We used semiquantitative PCR of the somatic Vα14-Jα18 rearrangement to confirm that the iNKT proportion was significantly reduced (Supplemental Figure 1E). Next, we used FACS analysis to quantify the apoptotic features of iNKTs in annexin V assays. We found no differences in terms of early apoptotic markers between the iNKTs from the livers of mutant mice and those of control mice, indicating that apoptosis does not account for the lower proportion of iNKTs found in mutant mice (Supplemental Figure 1F).

We then characterized the liver microenvironment in β-catenin–induced liver tumors. Relative to the other immune cell populations in the NPC compartment of β-catenin–activated tumors of Lpk-myc^{+} mice, iNKTs exhibited disproportionate decreases, which were similar to those found in the *Apc*$^{-/-}$ mice (Figure 2D and Supplemental Figure 1C).

To ascertain whether this iNKT population decrease was related to the activation of β-catenin signaling, we analyzed a transgenic HCC mouse model that undergoes β-catenin–independent tumorigenesis (21). In this model, the proportion of iNKT cells in the NPC population in the tumor microenvironment of SV40 T–induced HCC tumors was not lower than that found in control animal livers (Figure 2E and Supplemental Figure 1D).

Characterization of iNKT cells in β-catenin–activated livers. At least 2 phenotypically distinct subsets of iNKT cells exist in the liver and in other tissues of mice. These are defined as CD4^{+}CD8^{-} (CD4^{+}) and CD4^{-}CD8^{-} (double negative). We determined whether β-catenin activation had an impact on these 2 distinct subsets and found that the diminished proportion of iNKTs was more pronounced in the CD4^{+} iNKT cells than in the CD4^{-} iNKT cells (Figure 2C).

We then investigated the activation status of these cells by analyzing the cell surface levels of the constitutively expressed early activation marker CD69 in the livers of *Apc*$^{-/-}$ and control mice after tamoxifen treatment. We found that the iNKT activation level was significantly higher in *Apc*$^{-/-}$ livers compared with that in control livers (Figure 3A). We also found that the CD4^{-} and CD4^{+} iNKT cells were similarly activated (Figure 3A).

To determine whether the iNKT cells in the *Apc*$^{-/-}$ mutant mice were activated in vivo, we challenged mice with a sublethal dose of concanavalin A (ConA). *Apc*$^{-/-}$ livers were highly sensitive to ConA-induced hepatitis, as shown by histological analyses of the *Apc*$^{-/-}$ livers and by the subsequent increases in the serum levels of aspartate amino transferase (AST) (Figure 3, B and C). These results confirmed that iNKT cells were also activated in *Apc*$^{-/-}$ livers in vivo.

A striking characteristic of iNKT cells is their ability to rapidly produce Th1-type (e.g., IFN-γ) and Th2-type (e.g., IL-4) cytokines in response to primary stimulation, suggesting an important and diverse role for these cells in immunoregulation. It was recently reported that the liver CD4^{-} iNKTs are capable of promoting tumor rejection through IFN-γ production (22). Thus, we measured their capacity to produce IFN-γ and IL-4 using ex vivo analysis (20). We found that the CD4^{-} and CD4^{+} subpopulations of iNKTs, isolated from *Apc*$^{-/-}$mutant livers, were both able to produce higher amounts of IFN-γ and IL-4 compared with iNKTs isolated from control livers (Figure 3D).

Together, these findings show that, consequent to the oncogenic activation of β-catenin in hepatocytes, a specific inflammatory microenvironment was built up that particularly and preferentially had an impact on iNKT cells.

β-catenin activation in hepatocytes triggers a proinflammatory program associated with the activation of NF-κB. To better understand how β-catenin could contribute to this specific shaping of the liver microenvironment, we studied the expression of several immune mediators. We took advantage of recently generated deep-sequencing data, which identified the transcriptional program triggered in the hepatocytes in response to oncogenic activation of β-catenin. These data report the fold changes in the mRNA levels of genes regulated by β-catenin in hepatocytes (RNA-seq) and the repertoire of the TCF4/β-catenin binding

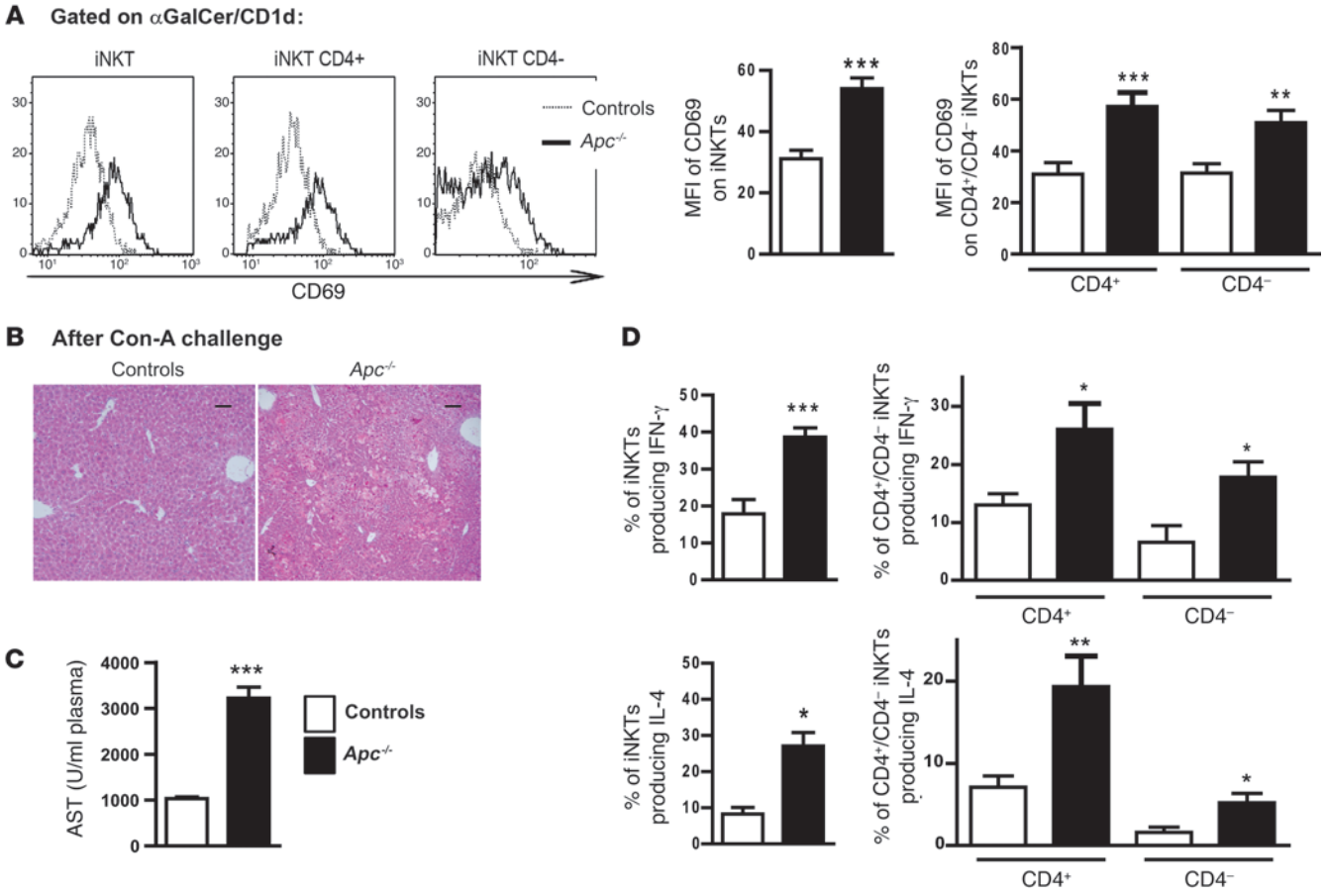

Figure 3

Characterization of iNKT cells in β-catenin–activated livers. NPCs were collected from livers 8 days after tamoxifen injection. (**A**) FACS profiles for CD69 expression (left panel) and MFI of CD69 (right panel) in NPCs gated on α-GalCer–loaded CD1d tetramer-positive cells (iNKTs) from *Apc*$^{-/-}$ and control livers, including those from the CD4$^+$ and CD4$^-$ subpopulations. (**B**) Paraffin-embedded sections obtained from control and *Apc*$^{-/-}$ livers after ConA challenge were stained with H&E. Scale bars: 50 μm. (**C**) Levels of AST were measured in the sera of control and *Apc*$^{-/-}$ mice 12 hours after ConA challenge. (**D**) Intracellular staining for IFN-γ (top panels) and IL-4 (bottom panels) was performed after in vitro stimulation of NPCs. This analysis was carried out in CD4$^+$ and CD4$^-$ α-GalCer/CD1d tetramer-positive cells. The graphs represent the percentage or the number of cells among the CD45$^+$Ly5$^+$ cells in the liver. The histograms are representative FACS analyses. All data are representative of 6 independent experiments with 5 mice/group. $^*P < 0.05$; $^{**}P < 0.01$; $^{***}P < 0.001$ (controls vs. *Apc*$^{-/-}$). Error bars represent SD.

sites within the hepatocyte chromatin (Chip-Seq), revealing whether or not these genes were direct targets of β-catenin (Torre et al., unpublished observations). Among the genes whose expression was modified including those that were or were not direct targets of β-catenin, we selected genes that were related to inflammation, and we performed real-time quantitative PCR (qPCR) on whole liver mRNA from the different mouse models we studied. As expected, Axin2 expression was strongly induced in preneoplastic *Apc*$^{-/-}$ liver and Lpk-myc$^+$ liver tumors, confirming the strong activation of β-catenin signaling in both models (Figure 4). We found that several proinflammatory chemokines and cytokines were upregulated, which could largely explain the immune cell recruitment in *Apc*$^{-/-}$ livers. Some of these genes were direct targets of β-catenin (e.g., *Ccl24*, *Cxcl2*, *Cxcl10*, *Cxcl11*, *Il15*, and *Il18*), and others were indirect target genes (e.g., *Ccl2* and *Ccl5*). However, we found that none of the genes encoding the canonical inflammatory mediators of liver inflammation, such as *Il6*, *Il1a*, *Il1b*, and *Tnfa*, were induced (Figure 4).

Together, the gene expression profiles of these livers argued that β-catenin is able to induce an inflammatory program in *Apc*$^{-/-}$ livers (Figure 4). Interestingly, most of the inflammatory-related genes found to be induced in the livers of *Apc*$^{-/-}$ mice were similarly increased in β-catenin–activated liver tumors developed in Lpk-myc$^+$ mice. Minor differences likely reflected the different stages of tumorigenesis produced by the 2 models (Figure 4).

The gene expression signatures of these tumor models (upregulation of *Ccl2*, *Ccl5*, *Il15*, *Il1r1*, *Tlr*, tweak receptor, the kinase *Ikk*β and *Socs3*) (see Figure 4) prompted us to investigate whether 2 key signaling pathways of inflammation, NF-κB and STAT3, were involved in tumorigenesis. We found that NF-κB was strongly activated in the tamoxifen-treated/β-catenin–activated livers (Figure 5A). Supershift analysis revealed an activation of mostly RelA/p50 heterodimers (Figure 5B). Using immunoblot analysis, we detected no STAT3 pathway activation in the livers of *Apc*$^{-/-}$ mutant mice, in accordance with the fact that Socs3 was directly induced by β-catenin activation (Figure 4 and

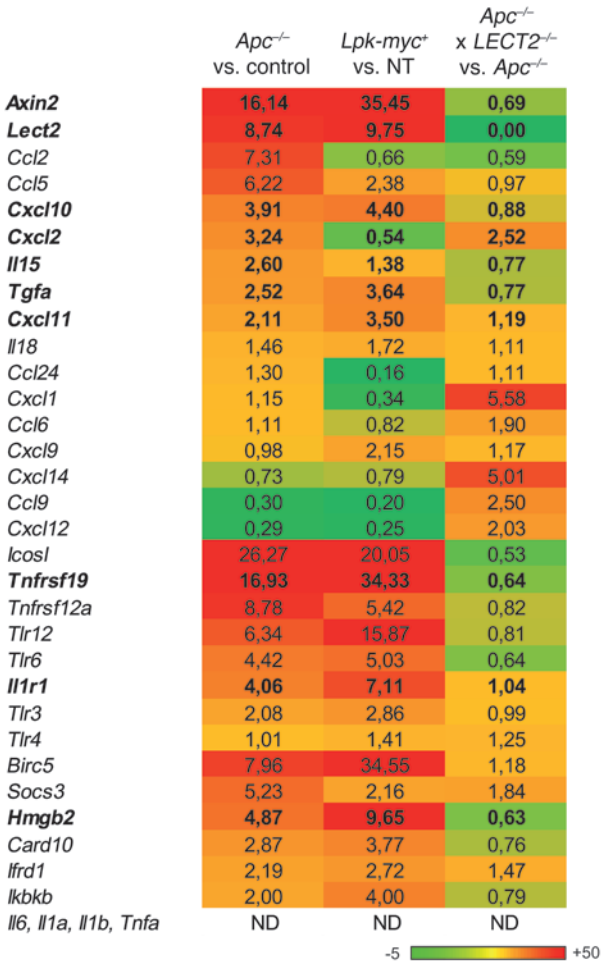

Figure 4
Inflammatory program induced in the liver by the oncogenic activation of β-catenin in the hepatocytes. Expression of different β-catenin target genes related to inflammation was analyzed using predesigned primers and probe sets from Applied Biosystems (Supplemental Table 1). Results are shown using a heat map visualization in which columns represent the different liver mouse samples studied and rows represent the various genes. Genes expressed at low levels are in green; those expressed at high levels are in red. ND, not detectable. Each group was composed of 4 mice.

Figure 5C). We found a similar level of NF-κB activation, with a lack of STAT3 activation, in the β-catenin–activated Lpk-myc$^+$ liver tumors (Figure 5, D and E).

We then analyzed chemokine and cytokine expression levels in the NPC compartment of *Apc*$^{-/-}$ and control livers to evaluate their production by the immune cells of the liver microenvironment. We found large increases in Ccl2, Ccl5, and Cxcl10 (Figure 5F) expression, and accordingly, higher levels of CCL5 were detected in the sera of *Apc*$^{-/-}$ mice (Figure 5G). However, none of the canonical liver inflammatory mediator genes *Il6*, *Il1b*, and *Tnfa* were induced in the NPC compartment of *Apc*$^{-/-}$ livers, emphasizing the singularity of β-catenin–induced liver inflammation (data not shown).

Together, our results indicate that oncogenic β-catenin signaling in hepatocytes is able to induce an inflammatory program that involves NF-κB, which through both autocrine and paracrine dialogues, leads to the remodeling of the liver microenvironment.

LECT2 exerts a critical role in shaping the inflammatory environment in β-catenin–activated livers. To identify soluble mediators involved in the control of the singular liver inflammatory milieu driven by β-catenin, we decided to investigate the role of LECT2, a secreted factor that we previously identified as a direct target gene of liver β-catenin (23). Although LECT2 function is still poorly characterized, it warranted investigation for several reasons. It is a chemokine-like protein that is involved in chemotaxis, cell proliferation, inflammation, and carcinogenesis (23–28). It was also one of the most upregulated genes in the β-catenin–induced inflammatory program expressed in the hepatocytes (Figure 4). It was also induced before the other chemokines/cytokines (see Supplemental Figure 2). Most importantly, *LECT2*-deficient mice harbor, in the liver, elevated numbers of iNKT cells (27), the component of the immune system that we found particularly targeted in β-catenin–induced liver inflammation.

To study the role of LECT2 in our HCC model, we generated mice lacking both Apc and LECT2 (*Apc*$^{-/-}$*LECT2*$^{-/-}$) and analyzed the inflammatory response induced in the absence of LECT2. First, we determined whether the Wnt/β-catenin pathways in the livers of the double-mutant mice and *Apc*$^{-/-}$ mice were triggered in similar manners (Figure 6A and Supplemental Figure 2). Macroscopic analysis of double-mutant mouse livers showed a particularly flaccid and loose texture compared with samples from *Apc*$^{-/-}$ mice. Histological staining of liver sections revealed some necrotic areas associated with immune infiltrates (Figure 6, B–E). Accordingly, serum transaminase levels were higher in *Apc*$^{-/-}$*LECT2*$^{-/-}$ mice than in *Apc*$^{-/-}$ mice (Figure 6F). This correlated with increased liver apoptosis (Supplemental Figure 2) and a decrease in the survival rate of the animals (Figure 6F).

To better define the molecular mechanisms responsible for the aggravated liver phenotype in *Apc*$^{-/-}$*LECT2*$^{-/-}$ mice, we used FACS analysis to investigate the liver NPC populations of these mice compared with those of mice with *Apc*$^{-/-}$ and *LECT2*$^{-/-}$ backgrounds. As expected, we found that the number of iNKT cells increased in *LECT2*$^{-/-}$ livers compared with those of control mice (27), but was not modified after oncogenic activation of β-catenin in the double-mutant livers (Figure 6G). More interestingly, we found that iNKT cells were not recruited in *Apc*$^{-/-}$ livers that expressed a high level of LECT2 induced by β-catenin, in accordance with the previous described inhibitory role of LECT2 in the homing of iNKT cells toward the liver (Figure 6G and ref. 27). We then analyzed the activation level of the iNKT in β-catenin–activated livers and found that the iNKTs were more activated in *Apc*$^{-/-}$*LECT2*$^{-/-}$ livers than in *Apc*$^{-/-}$ livers (Figure 6I). Moreover, their cytokine secretion profile was modified. Indeed, we detected a cytokine shift especially in the CD4$^-$ iNKT subpopulation, as they produced significantly less IFN-γ but far more IL-4 than the CD4$^-$ iNKT cells of *Apc*$^{-/-}$ livers (Figure 6J). As IFN-γ is a key antitumoral cytokine, our data suggested that the antitumoral properties of CD4$^-$ iNKTs in the absence of LECT2 were severely impaired.

In addition, we found that the profile of infiltrating immune cells in *Apc*$^{-/-}$*LECT2*$^{-/-}$ livers was characterized by an increase in neutrophils compared with those of *Apc*$^{-/-}$ mice (Figure 6H). In agreement with this finding, chemokines in the liver, such as *Cxcl1*, *Cxcl12*, and *Cxcl14*, were induced to higher levels in the *Apc*$^{-/-}$*LECT2*$^{-/-}$ mutant mice than in the *Apc*$^{-/-}$mutant mice (Figure 4). These results demonstrate that these 2 mutant backgrounds differed with respect to their infiltrating immune cell profiles and their chemokine/cytokine expression profiles.

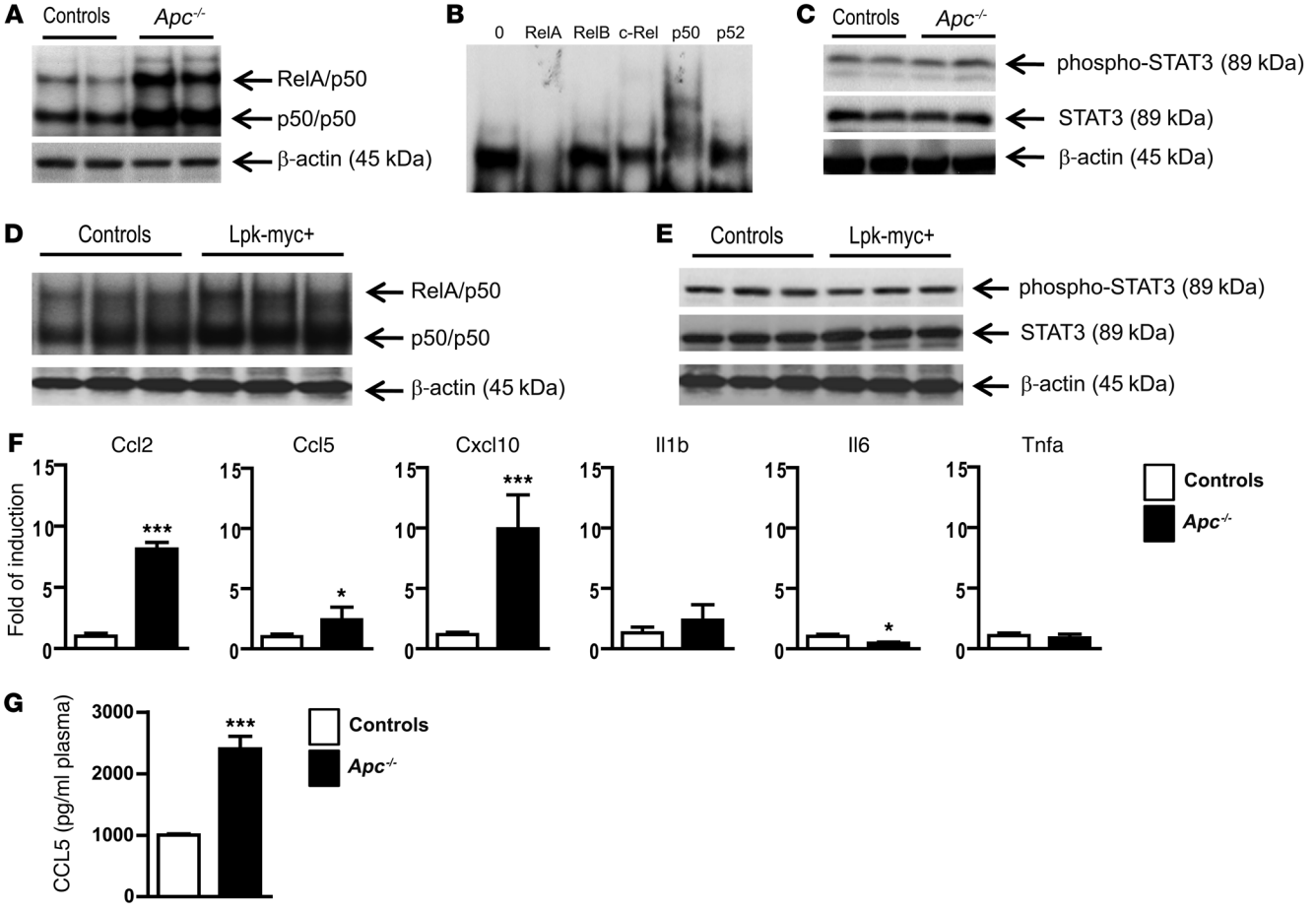

Figure 5

β-catenin activation in hepatocytes triggers an intrinsic inflammatory program associated with the activation of NF-κB. (**A**–**E**) NF-κB activation (**A**) in liver nuclear extracts from *Apc*$^{-/-}$ and control livers was monitored by EMSA analysis. Supershift analysis (**B**) was performed to determine which NF-κB subunit was involved in *Apc*$^{-/-}$ livers. Immunoblotting was used to detect phospho-STAT3, STAT3, and β-actin (**C**) in protein lysates from *Apc*$^{-/-}$ and control livers. NF-κB activation (**D**) in liver nuclear extracts from Lpk-myc^{+} and control livers was monitored by EMSA analysis. (**E**) Immunoblotting was used to detect phospho-STAT3, STAT3, and β-actin in protein lysates from Lpk-myc^{+} and control livers. (**F**) mRNAs were extracted from NPCs and analyzed by real-time qPCR using specific primers. (**G**) Sera from *Apc*$^{-/-}$ and control mice were collected and CCL5 plasma levels were evaluated using Luminex technology (Bio-Rad). All data with statistical analysis are representative of 4 experiments with 4 mice/group. $^{*}P < 0.05$; $^{***}P < 0.001$ (controls versus *Apc*$^{-/-}$). Error bars represent SD.

We next investigated NF-κB and STAT3 pathways in these mutant mice and found that NF-κB activation in *Apc*$^{-/-}$*LECT2*$^{-/-}$ livers was slightly lower than that in the *Apc*$^{-/-}$ livers, but that neither background exhibited any STAT3 activation (Figure 6K).

These findings revealed that LECT2 holds an important liver antiinflammatory property and appears to be an important player in modulating the intensity of the liver inflammatory immune response precipitated by oncogenic activation of β-catenin signaling in hepatocytes.

iNKT cells display antiinflammatory properties during β-catenin–induced liver inflammation. Since we confirmed a key role for LECT2 in iNKT cell homeostasis, we analyzed the role of these immune cells in β-catenin–induced liver inflammation. Using anti-NK1.1 antibodies, we depleted iNKT cells in *Apc*$^{-/-}$ livers and observed a strong increase in the inflammatory response compared with that in *Apc*$^{-/-}$ mutant mice injected with isotype-matched irrelevant antibodies (Figure 7, A and B). This was evidenced by the occurrence of large necrotic areas in the liver parenchyma, which were associated with increases in serum AST levels (Figure 7, B and C). FACS analysis showed that the subpopulation of immature inflammatory macrophages expressing F4/80^{+}CD11b^{+}Gr1^{+} had increased in the *Apc*$^{-/-}$ mutant iNKT-depleted livers compared with those in *Apc*$^{-/-}$mice treated with control antibodies (Figure 7D).

Therefore, we identified 2 interconnected effectors of the particular β-catenin–induced liver inflammation, the chemokine-like protein LECT2 and iNKT cells. Together, these effectors exerted antiinflammatory activities and dampened the magnitude of the liver inflammatory response driven by oncogenic activation of β-catenin in the hepatocytes.

iNKTs and LECT2 are critical cellular and molecular effectors controlling tumor progression of β-catenin–induced HCC. Finally, as we found that both depletion of the iNKT cells and deletion of LECT2 aggravated the inflammatory phenotype of *Apc*$^{-/-}$ livers, we evaluated their impact on β-catenin–dependent tumor development. We

generated Lpk-myc$^+$ mice either deficient in iNKTs using *Jα18*-KO animals (29) (Lpk-myc$^+$*Jα18*$^{-/-}$) or deficient in LECT2 (27) (Lpk-myc$^+$*LECT2*$^{-/-}$). We compared the development of liver tumors at 12 months in these 2 double-mutant mice to that in the Lpk-myc$^+$ single-mutant mice.

The absence of either iNKTs or LECT2 strongly promoted the progression of the HCC tumoral development induced by β-catenin (Figure 8, A and B). The number and size of tumor nodules in Lpk-myc$^+$*Jα18*$^{-/-}$ and in Lpk-myc$^+$*LECT2*$^{-/-}$ mice were greater than in Lpk-myc$^+$ control mice (Figure 8, A–I). The tumors that developed in the 2 types of double-mutant mice had higher grades of malignancy and were less differentiated than those of Lpk-myc$^+$ control mice (Figure 8, C–I). A number of tumors in the double-mutant animals exhibited a very poorly differentiated phenotype (fetal-like phenotype) that was never encountered in Lpk-myc$^+$ tumors (Figure 8, C–I). In addition, liver tumors from Lpk-myc$^+$*Jα18*$^{-/-}$ and Lpk-myc$^+$*LECT2*$^{-/-}$ mice had higher mitotic indices compared with tumors from Lpk-myc$^+$ mice (Figure 8, J and K). These results showed that the genetic deletion of either iNKTs or LECT2 strongly promoted both the initiation and progression steps of HCC development and led to a more undifferentiated phenotype. Remarkably, we found that 40% of the double-mutant mice harbored lung metastasis, a feature that was never observed in the Lpk-myc$^+$ mice (Figure 8L). Lung metastases were dramatically more prevalent in the mice that lacked iNKT cells than in the mice lacking LECT2 (Figure 8L).

Together, our findings provide strong evidence that, through the control of 2 interconnected inflammatory components, iNKT cells and the chemokine-like factor LECT2, β-catenin signaling induces an immune response that determines the aggressiveness of the tumorigenesis driven by β-catenin in hepatocytes.

Discussion

Using different genetically modified mouse models, we investigated whether β-catenin pathway activation, one of the most frequent events found in human HCC, induces a specific inflammatory microenvironment that could be involved in the oncogenic process. Our main finding is that β-catenin triggered a smoldering inflammation through the control of both pro- and antiinflammatory programs that was permissive for tumor development. The essence of the immune response determines tumor progression and metastatic capabilities.

We found that β-catenin induces a specific inflammatory program. Strikingly, the classical liver inflammatory cytokines described in a number of HCC-linked liver inflammation models, such as IL-6, TNF-α, IL-1α, and IL-1β (for review, see refs. 3, 4), were absent from the chemokine/cytokine profile induced by β-catenin activation in hepatocytes. The inflammatory program controlled by β-catenin and the singular inflammatory response that we described in this study constitute specific hallmarks of the inflammatory fuel induced by β-catenin in the liver. Our Chip-Seq data obtained from isolated hepatocytes revealed that several chemokine, cytokine, and cytokine receptor genes (e.g., *Lect2*, *Cxcl2*, *Cxcl10*, *Cxcl11*, *Il1*, and *Il1r1*) are cell-autonomous direct targets of β-catenin activation through the LEF/TCF motifs present in their promoters. Furthermore, we also observed a strong constitutive activation of NF-κB in the livers of *Apc*$^{-/-}$ mutant mice as well as in β-catenin–activated tumors. The increased expression of the chemokine/cytokine genes *Ccl2*, *Ccl5*, and *Il15*, all of which are bona fide NF-κB targets, probably results from this NF-κB activation. Thus, the proinflammatory chemokine/cytokine program arose from a combination of direct control by Wnt/β-catenin signaling and indirect control through NF-κB activation. The NF-κB activation likely resulted as a consequence of the cytokines produced by the immune cells and from β-catenin–induced increases in the expression levels of partners in the NF-κB pathway (such as *Il1r1* and *Il15*). As observed in other models of cancer-related inflammation (3), a feed-forward loop between the β-catenin–activated hepatocytes and the immune/inflammatory cells is likely to exist, and this could sustain tumor-associated inflammation (see Figure 9).

The induction of an intrinsic proinflammatory transcriptional program has been described for several other oncogenes, such as Ras and Myc family members, and constitutes a part of their oncogenic properties (3). What we believe is new in our findings is that we clearly demonstrate that β-catenin signaling is able to induce simultaneously a pro- and an antiinflammatory program that shapes a protumorigenic microenvironment with a low grade of chronic inflammation. We identified at least 2 interconnected mediators that could explain how β-catenin could induce a smoldering inflammation: a molecular mediator, LECT2, which is a chemokine-like protein that regulates the function of the cellular mediator, and the iNKT cells. Indeed, deletion of LECT2 resulted in a dramatic aggravation of the inflammatory response observed in the liver of *Apc*$^{-/-}$ mutant mice. The antiinflammatory functions of LECT2 have been reported to play a suppressive role in anti–type II collagen antibody–induced arthritis (30). The precise mechanism by which LECT2 exerts an antiinflammatory action in the liver is presently unknown, but our results provide some clues. Analysis of *LECT2*-deficient animals demonstrated that LECT2 regulates iNKT cell homeostasis in the liver through at least 2 nonexclusive mechanisms: (a) the control of iNKT homing activity toward the liver and (b) the control of the iNKT Th1/Th2 cytokine secretion profile (27). Our data strongly support the notion that LECT2 controls the homing of the iNKT in β-catenin–activated livers. As expected (27), the number of iNKT cells in these livers increased in *LECT2*-deficient mice, suggesting that LECT2 prevents iNKT homing toward the liver. In addition, iNKT cells were not recruited to the livers of *Apc*$^{-/-}$ mutant mice, which retain the ability to produce high levels of LECT2 induced by β-catenin. In contrast, most other immune cell populations were actively recruited to this β-catenin–induced liver microenvironment. These observations support the view that LECT2 prevents the homing of the iNKTs toward the liver. In addition, the numbers of iNKT cells in *Apc*$^{-/-}$*LECT2*$^{-/-}$ livers and in the livers of *LECT2*$^{-/-}$ mice were the same, showing the key role of LECT2 in iNKT cell homing. Corroborating the present data, we recently found that the number of iNKT cells in the livers of mice that harbored a hepatospecific deletion of β-catenin and lacked LECT2 expression increased following tamoxifen treatment, revealing that these mice have an immune phenotype similar to that of *LECT2*-deficient mice (J.P. Couty and S. Colnot, unpublished observations). Furthermore, we found that iNKTs were more highly activated in *Apc*$^{-/-}$*LECT2*$^{-/-}$ mice than in *Apc*$^{-/-}$ mice, but exhibited an altered cytokine secretion profile. This was more pronounced in the CD4$^-$ iNKT subpopulation, which had shifted toward a Th2 phenotype. The CD4$^-$ iNKT subpopulation has been reported to display potent antitumoral activities through its production of high levels of IFN-γ. Thus, the shift in its cytokine secretion profile to lower levels of IFN-γ is consistent with the higher grade of malignancy observed in Lpk-myc$^+$*LECT2*$^{-/-}$ mice compared with that found in Lpk-myc$^+$ mice.

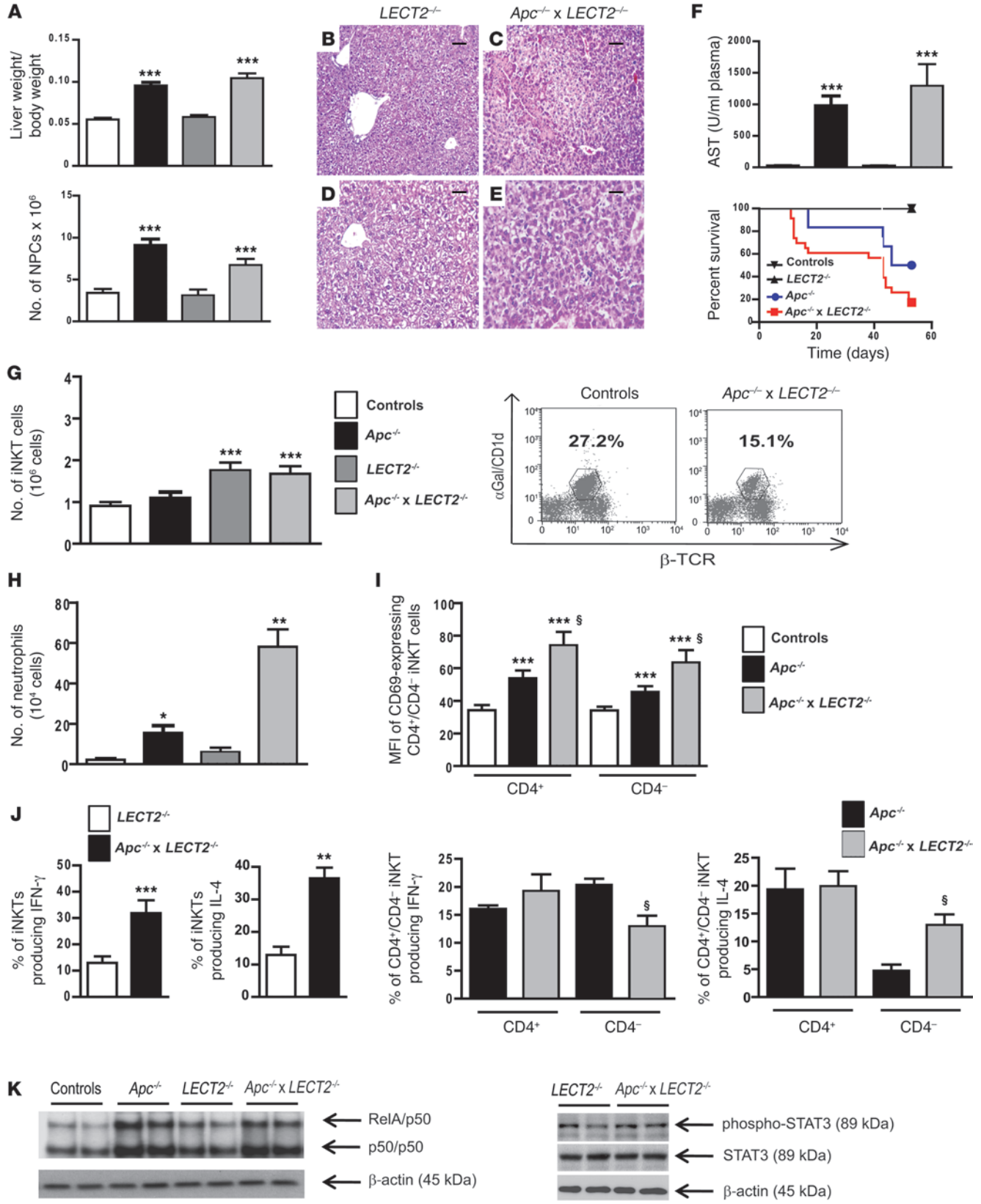
A
Liver weight/ body weight
No. of NPCs x 10^6
B
C
D
E
LECT2-/-
Apc-/- x LECT2-/-
F
AST (U/ml plasma)
Percent survival
Controls
LECT2-/-
Apc-/-
Apc-/- x LECT2-/-
Time (days)
G
No. of iNKT cells (10^6 cells)
Controls
Apc-/-
LECT2-/-
Apc-/- x LECT2-/-
αGal/CD1d
27.2%
15.1%
β-TCR
H
No. of neutrophils (10^4 cells)
I
MFI of CD69-expressing CD4+/CD4- iNKT cells
CD4+
CD4-
J
% of iNKTs producing IFN-γ
% of iNKTs producing IL-4
% of CD4+/CD4- iNKT producing IFN-γ
% of CD4+/CD4- iNKT producing IL-4
K
Controls
Apc-/-
LECT2-/-
Apc-/- x LECT2-/-
RelA/p50
p50/p50
β-actin (45 kDa)
phospho-STAT3 (89 kDa)
STAT3 (89 kDa)

Figure 6
LECT2 has a critical role in shaping the inflammatory environment in β-catenin–activated liver. (**A**) The ratio of liver/body weights and the number of NPCs were evaluated in controls, *Apc*$^{-/-}$, *LECT2*$^{-/-}$, and *Apc*$^{-/-}$ × *LECT2*$^{-/-}$ livers 8 days after tamoxifen injection. (**B**–**E**) Paraffin-embedded livers sections from the same group of mice were stained with H&E. Scale bars: 100 μm (**B** and **C**); 60 μm (**D** and **E**). (**F**) Serum AST levels (upper panel) and Survival curves (lower panel) were assessed in the same conditions. (**G**) FACS analysis of NPCs using α-GalCer–loaded CD1d tetramers and anti-TCR β chain staining to assess the number (left panel) and proportion (right panel) of iNKT cells in the livers of the same mice groups. (**H**) FACS analysis of NPCs using anti-Ly6G staining to assess the number of neutrophils. (**I**) MFI of CD69$^+$ cells in NPCs gated on iNKTs. (**J**) Intracellular staining for IFN-γ and IL-4 were performed after in vitro stimulation for total (left panel) and CD4$^+$ or CD4$^-$ iNKTs (right panel). (**K**) Nuclear NF-κB activation from *LECT2*$^{-/-}$ and *Apc*$^{-/-}$ × *LECT2*$^{-/-}$ livers was monitored by EMSA. Immunoblotting of phospho-STAT3, STAT3, and β-actin on protein lysates. All data with statistical analysis are representative of 4 experiments with 5 mice/group. $^*P < 0.05$; $^{**}P < 0.01$; $^{***}P < 0.001$ (controls versus *Apc*$^{-/-}$ or *LECT2*$^{-/-}$ versus *Apc*$^{-/-}$*LECT2*$^{-/-}$); $^{\S}P < 0.03$ (*Apc*$^{-/-}$ versus *Apc*$^{-/-}$ × *LECT2*$^{-/-}$). Error bars represent SD.

Depletion of iNKT cells by anti-NK1.1 antibodies markedly aggravated the inflammatory response observed in the livers of *Apc*$^{-/-}$ mutant mice in a manner similar to that produced by *Apc*$^{-/-}$ mice lacking the *LECT2* gene. iNKTs are a specific population of immune T cells that are particularly enriched in the liver (31). There is compelling evidence that iNKT cells have an important role in tumor immunosurveillance in mice (32). The CD4$^-$ iNKT cell subset appears to be responsible for the main antitumoral response through its production of IFN-γ. The cytokine profile of CD4$^-$ NKTs in humans indicates that they might have a similar role (22, 33, 34). iNKT cells from patients with cancer have been shown to produce less IFN-γ than iNKT cells from healthy individuals (35, 36). Our results correlated with these observations, since genetic deletion of the iNKT cells in Lpk-myc$^+$*Jα18*$^{-/-}$ mice led to a stronger progression of β-catenin–activated tumors. Our results provide some clues to explain how iNKTs exert their antitumoral properties. By dampening the inflammatory response (adequate immune response) and by controlling the composition of the inflammatory milieu through immunosuppressive effectors, iNKTs might prevent the tumor microenvironment from becoming permissive to the metastatic process. We found that the number of a subpopulation of immature inflammatory macrophages expressing F4/80$^+$ CD11b$^+$ Gr1$^+$ was higher in iNKT-depleted *Apc*$^{-/-}$ livers compared with the livers of *Apc*$^{-/-}$ mice treated with control antibodies. These inflammatory macrophages were recently identified in inflammation-induced colorectal tumorigenesis and were reported to be a major source of tumor-promoting factors (37).

Another important implication of our results is that β-catenin signaling appears to determine the metastatic spread of β-catenin–mutated HCCs by controlling the level of inflammation. Genetic deletion of either LECT2 or the iNKT cells in Lpk-myc$^+$ mice caused β-catenin–induced HCCs to progress into high-grade tumors, and in almost half of mice, these produced lung metastases. As both LECT2 and the iNKT cells displayed antiinflammatory properties, these results highlight the critical role of the magnitude of the inflammatory response as a driving force in cancer metastasis. The mechanisms involved need further investigation, but 2 of the chemokines that were upregulated in *LECT2*-deficient mice, CXCL1 and CXC12, have already been implicated in metastasis (38, 39).

Finally, our data are sharply relevant to human HCC pathogenesis. Constitutive activations of NF-κB and STAT3 have been described in human HCCs (40). Although the β-catenin genetic status of these tumors was not determined, these authors found an inverse relationship between NF-κB and STAT3 and also found that the majority of STAT3-positive HCCs were negative for NF-κB activation. NF-κB–positive tumors were also found to be less aggressive than the STAT3-positive tumors (40). Our data showing that β-catenin–activated tumors, as well as those in the livers of tamoxifen-treated *Apc*$^{-/-}$mice, displayed NF-κB pathway activation, but not STAT3 pathway activation, are in perfect correlation with the human study (40). In addition, constitutive activation of the STAT3 pathway leads to the development of benign adenomas that progress to HCC only when it is combined with β-catenin–activating mutations (41). This observation reinforces our results that oncogenic β-catenin activation did not result in constitutive STAT3 activation, and may explain why β-catenin gain-of-function mutations are required for the progression of STAT3-activated liver adenoma to HCC. Finally, since the immune response in the presence of LECT2 retained antitumor activity, our results suggest that the particular inflammatory program induced by β-catenin that results in low-level inflammation may be part of the reason why β-catenin–activated human HCCs belong to a subclass of HCCs with rather better prognoses than other HCCs (see Figure 9). A second point is that, in a previous study, we found that LECT2 expression levels in β-catenin–activated human HCCs inversely correlated with the differentiation status of the tumor (23). Consistent with our present data, LECT2 transcripts were found to be downregulated in HCC patients with vascular invasion, again suggesting that LECT2 has tumor suppressor functions (26). The reasons that LECT2 is downregulated in human HCCs is still unknown, but the results of a recent study indicate that it could be linked to an epigenetic mechanism (42). In their investigation of the role of a methyl-binding domain protein (Mbd2) in Wnt signaling, the authors found that the *Lect2* gene was the only β-catenin target gene that was upregulated in an Mbd2 deficiency context. All other β-catenin target genes whose expression was modified in Mbd2 deficiency were downregulated (42).

Our data identified inflammation as a new player of β-catenin–induced liver tumorigenesis and showed that oncogenic β-catenin signaling constructed a permissive inflammatory environment that had an impact on HCC development. LECT2 and iNKT cells are potentially new targets in immunotherapeutic approaches to the treatment of liver cancer.

Methods

Mice. All mice were kept in well-controlled animal housing facilities and had free access to tap water and food pellets. Mice capable of an inducible inactivation of the *Apc* gene in the hepatocytes have been described previously (14, 15). Briefly, mice carrying the *Apc* gene flanked by loxP sequences were crossed with transthyretin TTR-Cre-Tam mice (43) to generate *Apc*$^{-/-}$ (*Apc*$^{flox/flox}$, TTR-Cre-Tam) and control mice (*Apc*$^{flox/flox}$, Cre negative). *Apc*$^{-/-}$ mutant mice were bred on a C57BL/6 background for at least 6 generations before the different strains were crossed. L-type pyruvate kinase Lpk-myc$^+$ transgenic mice, which express the oncogene c-myc in the liver under the control of rat L-PK regulatory regions and develop multifocal HCCs, were bred on a C57BL/6 background for at least 8 generations before being crossed (9). *LECT2*-deficient mice (*LECT2*$^{-/-}$) were provided by S. Yamagoe (27) and were backcrossed for 10 generations on a C57BL/6 background. *Apc*$^{-/-}$ mice were crossed with *LECT2*$^{-/-}$ mice to gen-

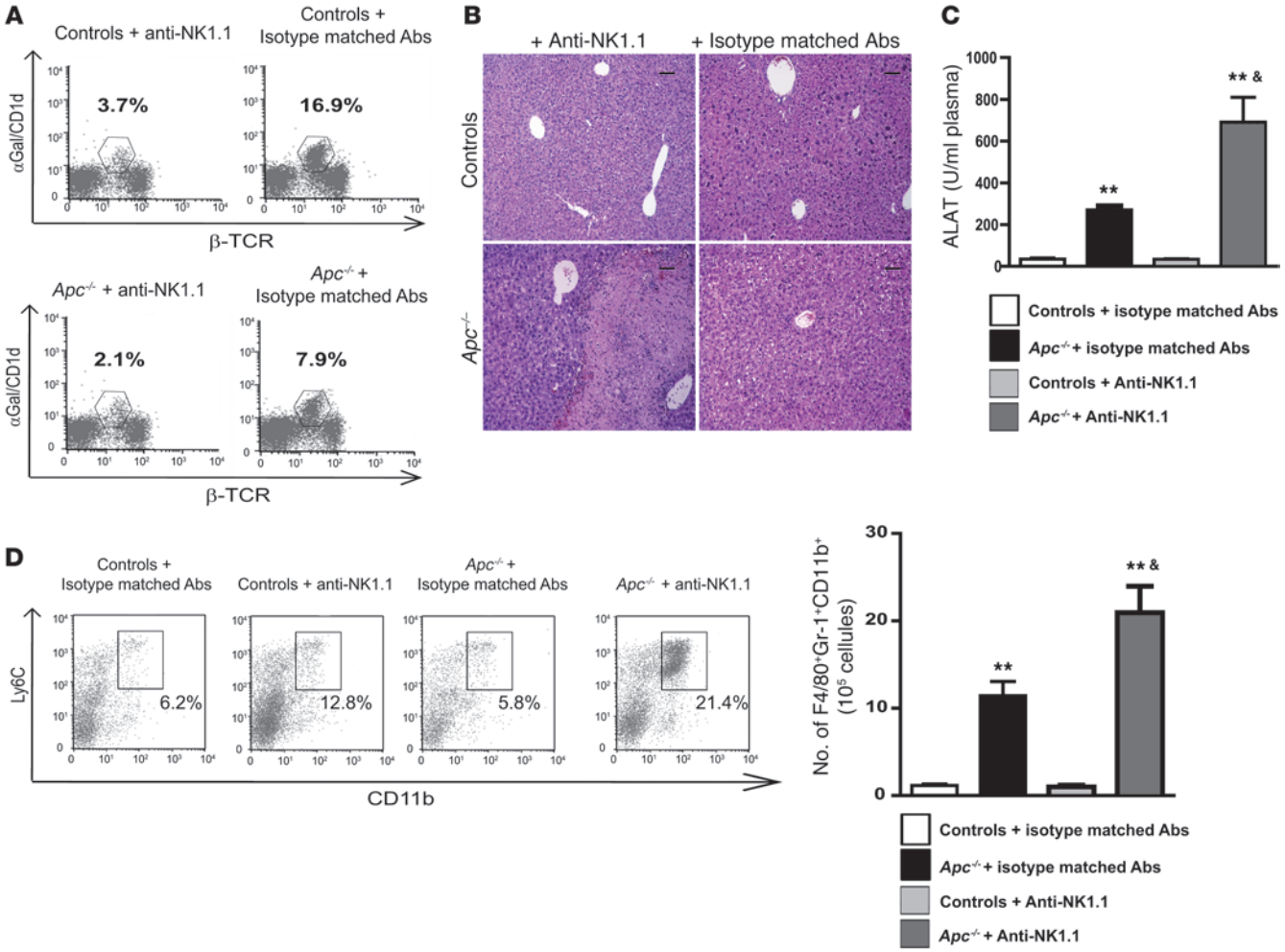

Figure 7

iNKTs display antiinflammatory properties during β-catenin–induced liver inflammation. (**A**) FACS analysis of NPCs was performed to assess iNKT cell depletion in controls and *Apc*$^{-/-}$ livers after treatment with anti-NK1.1 or isotype-matched irrelevant antibodies 8 days after tamoxifen injection. (**B**) Paraffin-embedded sections obtained from controls and *Apc*$^{-/-}$ livers after treatment with anti-NK1.1 or isotype-matched irrelevant antibodies were stained with H&E. Scale bars: 50 μm. (**C**) Serum transaminase levels (ALAT) were measured in controls and *Apc*$^{-/-}$ mice after treatment with anti-NK1.1 or isotype-matched antibodies. (**D**) The sub-populations of F4/80$^+$CD11b$^+$Ly6C$^+$ immature macrophages were quantified in the livers of *Apc*$^{-/-}$ and control mice treated with either anti-NK1.1 or isotype-matched irrelevant 8 days after tamoxifen injection. Dot plots show representative FACS analyses of immature macrophages, gated on F4/80$^+$ cells. The numbers indicate the percentage of these cells among the F4/80$^+$ cells. All data are representative of 3 independent experiments with 4 mice/group. $^{**}P < 0.01$ (controls vs. *Apc*$^{-/-}$); $^{\&}P < 0.01$ (*Apc*$^{-/-}$ + isotype-matched Abs versus *Apc*$^{-/-}$ + anti-NK1.1 Abs).

erate *Apc*$^{-/-}$*LECT2*$^{-/-}$ (*Apc*$^{flox/flox}$, TTR-Cre-Tam, *LECT2*$^{-/-}$), *Apc*$^{-/-}$ (*Apc*$^{flox/flox}$, TTR-Cre-Tam, *LECT2*$^{+/+}$) and their respective controls (*Apc*$^{flox/flox}$, Cre-negative *LECT2*$^{-/-}$; *Apc*$^{flox/flox}$, Cre-negative *LECT2*$^{+/+}$). All 7- to 9-week-old mice received a single i.p. injection of 1.5 mg of tamoxifen (MP Biomedicals). Lpk-myc$^+$ mice were crossed with *LECT2*$^{-/-}$ mice to generate double Lpk-myc$^+$*LECT2*$^{-/-}$ and control single Lpk-myc$^+$ mice (Lpk-myc*LECT2*$^{+/+}$). Lpk-myc$^+$ mice were crossed with *Jα18*$^{-/-}$ (deficient in iNKTs and backcrossed for 13 generations on a C57BL/6 background) mice (29) to generate double Lpk-myc$^+$*Jα18*$^{-/-}$ and control single Lpk-myc$^+$ mice (Lpk-myc*Jα18*$^{+/+}$). Tumor development was studied at 12 months in control single Lpk-myc$^+$ and double Lpk-myc$^+$*LECT2*$^{-/-}$ or Lpk-myc$^+$*Jα18*$^{-/-}$ mice. Only littermates were used to constitute homogeneous groups of mice.

Nonparenchymal liver cell preparation. Livers were harvested and then perfused with 1× HBSS containing 10 mM HEPES to remove circulating blood cells. The liver was passed through a stainless steel mesh in RPMI 1640 supplemented with 2% heat-inactivated FCS (JRH Biosciences), 5 mM HEPES, 2 mM GlutaMAX (Invitrogen; Life Technologies), 100 U/ml penicillin, 100 μg/ml streptomycin, and 510^{-5} M β-mercaptoethanol (Sigma-Aldrich). The liver cell suspension was collected, and parenchymal cells were separated from NPCs by centrifugation for 2 minutes at 48 *g*. The supernatant containing the NPCs was collected and centrifuged for 10 minutes at 440 *g*. The pellet was then resuspended in 40% percoll diluted in RPMI 1640 supplemented with 2% FCS, layered onto 80% percoll, and centrifuged for 15 minutes at room temperature at 780 *g*. The NPC fraction was collected at the interface (40%/80% percoll), and the cells were spun down twice in ice-cold PBS. Viable NPCs were counted by a trypan blue exclusion method, resuspended in serum-containing medium, and stored on ice until further use.

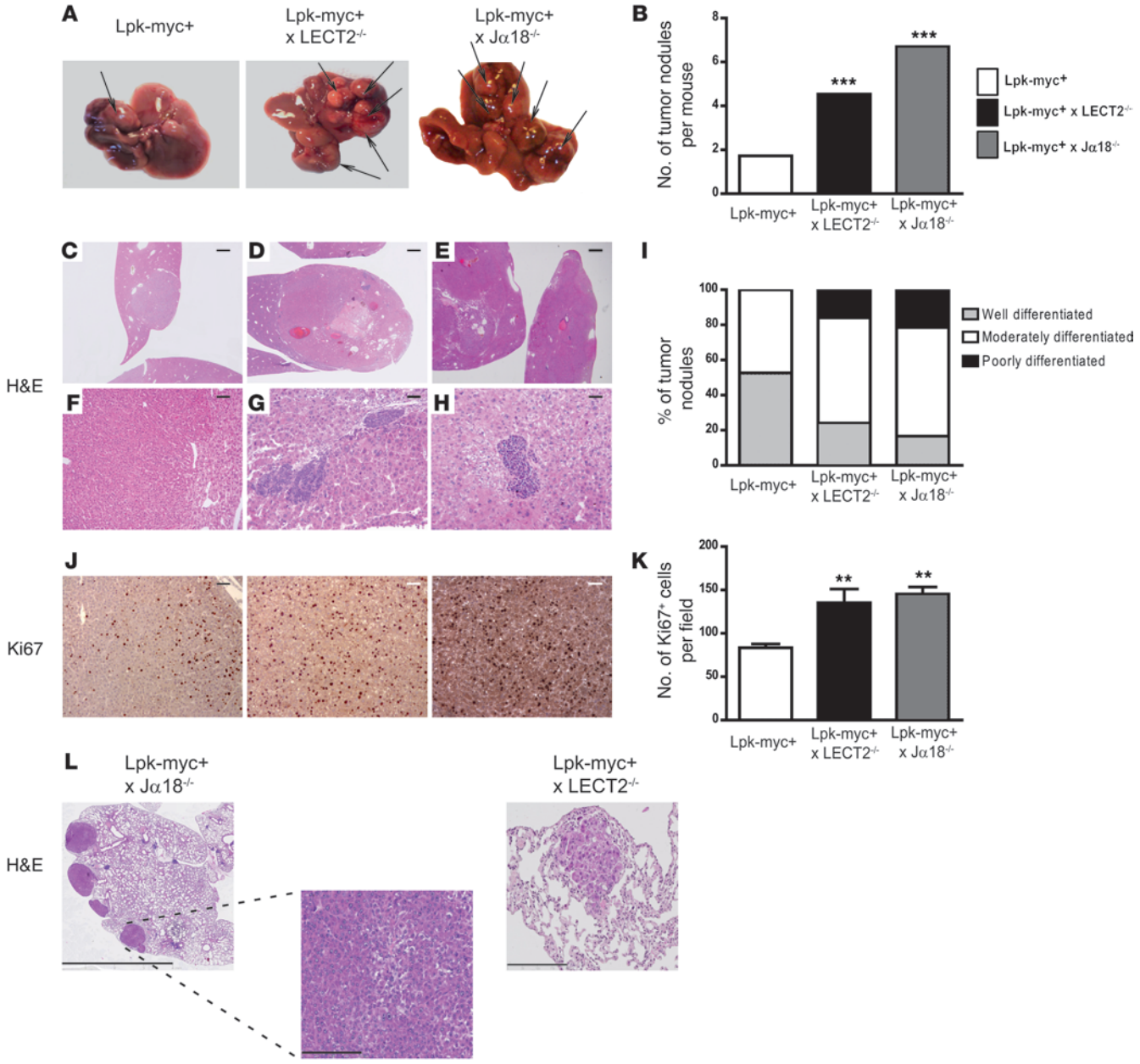

Figure 8

iNKTs and LECT2 are critical cellular and molecular players controlling tumoral progression of β-catenin–dependent liver tumorigenesis. (**A**) 12-month-old Lpk-myc$^+$ (n = 12) and Lpk-myc$^+$*LECT2*$^{-/-}$ (n = 11) or Lpk-myc$^+$*Jα18*$^{-/-}$ (n = 7) mice were sacrificed, and the number of tumor nodules was evaluated (arrows). (**B**) The graph represents the mean number of tumors for each group of mice. (**C**–**H**) Paraffin-embedded sections obtained from Lpk-myc$^+$, Lpk-myc$^+$*LECT2*$^{-/-}$, and Lpk-myc$^+$*Jα18*$^{-/-}$ livers were stained with H&E, and the grade of differentiation for each tumor nodule was assessed. Scale bars: 1 mm (**C**–**E**); 120 μm (**F**); 60 μm (**G** and **H**). (**I**) The graph shows the mean number of tumors for each group of mice, according to their degree of differentiation. (**J**) Immunohistochemistry of Ki67 expression was performed on paraffin-embedded sections obtained from Lpk-myc$^+$ and Lpk-myc$^+$*LECT2*$^{-/-}$ or Lpk-myc$^+$*Jα18*$^{-/-}$ livers to evaluate the proliferation rate of the tumor nodules. Scale bars: 50 μm. (**K**) The graph represents the mean number of Ki67$^+$ cells for each group of mice. (**L**) Paraffin-embedded sections obtained from Lpk-myc$^+$, Lpk-myc$^+$*LECT2*$^{-/-}$, and Lpk-myc$^+$*Jα18*$^{-/-}$ lungs were stained with H&E. Scale bars: 4 mm (left); 200 μm (middle, right).

Flow cytometry. Flow cytometry was performed on a FACSCalibur flow cytometer (BD Biosciences). Cells were incubated with anti-CD16/CD32 antibodies (Fcγ III/II receptor, clone 2.4G2) prior to staining with labeled antibodies (or isotype-matched control immunoglobulin) according to the manufacturer's recommendations. NPCs were identified according to cell surface expression of Ly5 to calculate the proportion and absolute numbers of immune cell subpopulations. We used the following monoclonal antibodies: anti–TCR-β chain, anti-NK1.1, anti-CD19, anti-Gr1, anti-CD4, anti-CD8, anti-CD69, anti-Ly6C, anti-Ly6G, anti-B220, and anti-CD45/Ly5, that were purchased from BD Biosciences and Pharmingen.

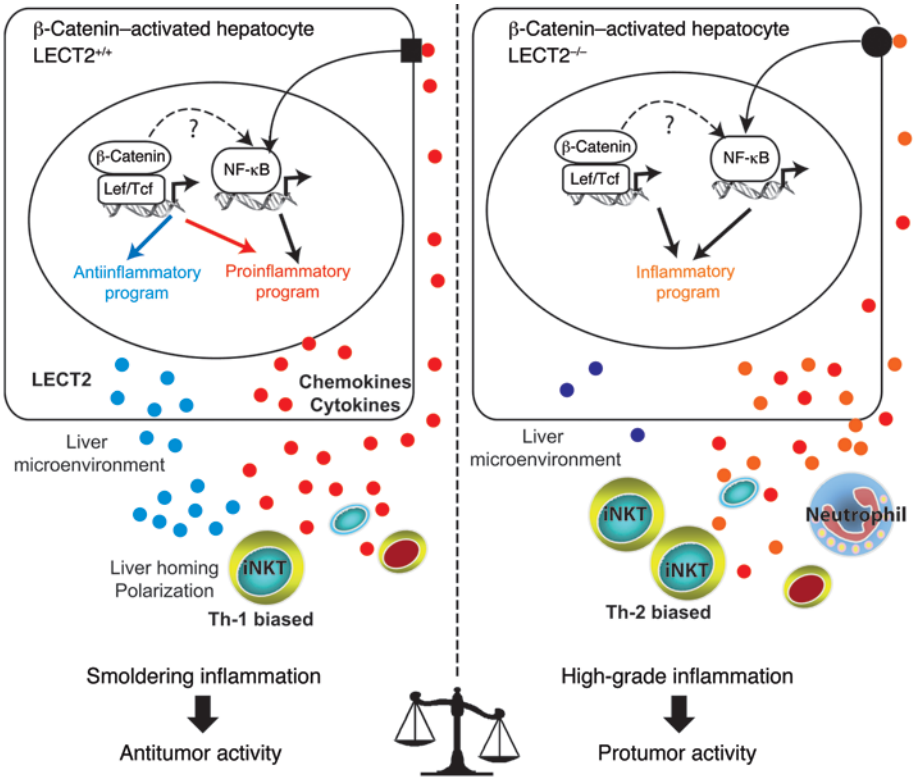

Figure 9
Liver inflammation is critical for β-catenin–induced liver tumorigenesis. Oncogenic activation of β-catenin in hepatocytes triggers an intrinsic inflammatory program with both pro- and antiinflammatory mediators that together construct an inflammatory microenvironment that controls tumor progression. In Apc-deficient (*Apc*$^{-/-}$) hepatocytes, β-catenin signaling is constitutively activated and induced: (a) the expression of a proinflammatory program resulting from both a direct control by the Wnt/β-catenin signaling and an indirect control by NF-κB that is not yet understood and (b) the expression of an antiinflammatory program including at least the direct LECT2 target gene. 2 interconnected factors relay the antiinflammatory response, the chemokine-like factor LECT2 and the iNKT cells. iNKT cell homeostasis is controlled by LECT2 at the level of liver homing and cytokine polarization. Together, the β-catenin–induced liver microenvironment exhibits a low grade of chronic inflammation that preserves an immune response with antitumor activity. In mice deficient in Apc and LECT2 (*Apc*$^{-/-}$*LECT2*$^{-/-}$), the lack of LECT2 causes high-grade inflammation in the liver microenvironment, which strongly potentiates the tumoral process and results in lung metastases (see Results).

Anti-F4/80-APC was purchased from eBiosciences. CD1d–α-galactosylceramide–loaded (CD1d–α-GalCer-loaded) tetramers (APC-labeled) were provided by the NIH Tetramer Core Facility. CELLQuest software (BD Biosciences) was used for analyzing flow cytometry data.

Intracellular staining. Liver NPCs were stimulated for 4 hours with 10^{-8} M of PMA (Sigma-Aldrich), 10^{-6} M ionomycin, and 10 μg/ml brefeldin A. Cells were then washed and incubated with CD1d–α-GalCer tetramer-APC, anti–NK1.1-PE, anti–β-TCR-FITC, and anti–CD4-PerCp. For intracellular staining, cells were fixed with 4% PFA, washed, and subsequently permeabilized using the Cytofix/Cytoperm BD kit following the manufacturer's instructions, and then further incubated with anti–IL-4 or anti–IFN-γ (both Alexa Fluor 488 or PE conjugated) (BD Biosciences). The cells were washed and analyzed on a FACSCalibur flow cytometer using CellQuest software (BD Biosciences).

Cell cycle analysis. Mice were injected i.p. with 50 mg/kg of BrdU (Sigma-Aldrich) and were killed 2 hours later. Incorporated BrdU was detected intracellularly using anti-BrdU FITC or APC-conjugated antibodies according to the manufacturer's recommendations (BD Biosciences).

ConA-induced liver injury. Mice were injected i.v. with 15 mg/kg ConA (Sigma-Aldrich) 8 days after Wnt/β-catenin triggering. Mice were killed 6–10 hours after ConA injection.

EMSA. Nuclear extracts were prepared and analyzed for DNA binding activity using the HIV-LTR tandem B oligonucleotide as a B probe as previously described (44). For supershift assays, nuclear extracts were incubated with specific antibodies for 30 minutes on ice before incubation with the labeled probe.

Histological studies. Liver biopsies were fixed and embedded in paraffin prior to staining with H&E. Immunostaining of glutamine synthase to monitor β-catenin activation was performed as previously described (14). Immunostaining of Ki67 (Novocastra) to monitor the proliferation of hepatocytes was performed as previously described (45).

Serum transaminase levels. Blood was collected and transaminase levels were measured by a standard method as previously described (46).

RNA extraction and analyses. Total RNAs were extracted with RNeasy kit (QIAGEN) and real-time qPCR analysis was performed using Taqman (Roche Diagnostics) as previously described (41). Gene expression was analyzed using TaqMan gene expression assays (Applied Biosystems) as described in Supplemental Table 1. Gene expression was normalized to ribosomal 18S RNA (41). The level of expression of all the inflammatory genes in the different mouse liver samples was calculated with the 2ΔΔCT method and compared with the expression level of the corresponding gene in control liver tissues and expressed as an *n*-fold ratio.

Cytokine assays. The chemokine CCL5 was quantified in mouse sera by Luminex technology and the Bio-Rad 9 Plex Kit, according to the manufacturer's recommendations (Bio-Rad).

Western blotting. Immunoblot analyses of liver protein extracts were performed using anti–phospho-STAT3, anti-STAT3, and anti–β-actin antibodies (Cell Signaling).

Study approval. All reported animal procedures were approved by the French Institutional Animal Care and Use Committee and by the Directeur départemental des Services Vétérinaires of the Prefecture de Police de Paris (Paris, France).

Statistics. Data are expressed as mean ± SD. Statistical significance was determined by 2-way ANOVA followed by a Student's *t* test. $P < 0.05$ was considered statistically significant.

Acknowledgments

We thank Beatrice Romagnolo, Catherine Cavard, and Hélène Gilgenkrantz for their expertise and critical reading of the manuscript. We are indebted to André Herbelin and the NIH Tetramer Facility (Bethesda, Maryland, USA) for providing us with α-GalCer–loaded tetramers. We thank Gabrielle Couchy for her technical expertise in TaqMan assays. We thank Masaru Taniguchi for providing *Jα18*-deficient mice (29). This study was supported by grants from the Centre National de la Recherche Scientifique (CNRS), Institut National de la Santé et de la Recherche Médicale (INSERM), the Ligue Nationale Contre Le Cancer (Equipe labellisée), Agence Nationale de Recherche (ANR) 07-Physiology and the Axe 3 of Canceropole Ile-de-France, Association Française des Etudes sur le Foie, Association Française des Etudes sur le Foie (AFEF), and the Laboratoire ROCHE.

Received for publication September 27, 2011, and accepted in revised form December 7, 2011.

Address correspondence to: Mireille Viguier or Christine Perret, Institut Cochin, INSERM U1016, UMR CNRS 8104, Université René Descartes, Département Endocrinologie, Métabolisme et Cancer, Bâtiment Faculté, 24, rue du Faubourg Saint-Jacques, 75014 Paris, France. Phone: 33.1.57.27.80.06; Fax: 33.1.57.27.80.87; E-mail: mireille.viguier@inserm.fr (M. Viguier). Phone: 33.1.44.41.25.64; Fax: 33.1.44.41.24.21; E-mail: christine.perret@inserm.fr (C. Perret).

1. de Visser KE, Coussens LM. The inflammatory tumor microenvironment and its impact on cancer development. *Contrib Microbiol*. 2006;13:118–137.
2. Mantovani A, Allavena P, Sica A, Balkwill F. Cancer-related inflammation. *Nature*. 2008; 454(7203):436–444.
3. Grivennikov SI, Greten FR, Karin M. Immunity, inflammation, and cancer. *Cell*. 2010;140(6):883–899.
4. Grivennikov SI, Karin M. Dangerous liaisons: STAT3 and NF-kappaB collaboration and crosstalk in cancer. *Cytokine Growth Factor Rev*. 2010;21(1):11–19.
5. El-Serag HB, Rudolph KL. Hepatocellular carcinoma: epidemiology and molecular carcinogenesis. *Gastroenterology*. 2007;132(7):2557–2576.
6. Crispe IN. The liver as a lymphoid organ. *Annu Rev Immunol*. 2009;27:147–163.
7. Luedde T, Schwabe RF. NF-kappaB in the liver--linking injury, fibrosis and hepatocellular carcinoma. *Nat Rev Gastroenterol Hepatol*. 2011;8(2):108–118.
8. Laurent-Puig P, et al. Genetic alterations associated with hepatocellular carcinomas define distinct pathways of hepatocarcinogenesis. *Gastroenterology*. 2001;120(7):1763–1773.
9. de La Coste A, et al. Somatic mutations of the beta-catenin gene are frequent in mouse and human hepatocellular carcinomas. *Proc Natl Acad Sci U S A*. 1998;95(15):8847–8851.
10. Miyoshi Y, et al. Activation of the beta-catenin gene in primary hepatocellular carcinomas by somatic alterations involving exon 3. *Cancer Res*. 1998;58(12):2524–2527.
11. Audard V, et al. Cholestasis is a marker for hepatocellular carcinomas displaying beta-catenin mutations. *J Pathol*. 2007;212(3):345–352.
12. Boyault S, et al. Transcriptome classification of HCC is related to gene alterations and to new therapeutic targets. *Hepatology*. 2007;45(1):42–52.
13. Chiang DY, et al. Focal gains of VEGFA and molecular classification of hepatocellular carcinoma. *Cancer Res*. 2008;68(16):6779–6788.
14. Benhamouche S, et al. Apc tumor suppressor gene is the "zonation-keeper" of mouse liver. *Dev Cell*. 2006;10(6):759–770.
15. Colnot S, et al. Liver-targeted disruption of Apc in mice activates beta-catenin signaling and leads to hepatocellular carcinomas. *Proc Natl Acad Sci U S A*. 2004;101(49):17216–17221.
16. de La Coste A, et al. Paradoxical inhibition of c-myc-induced carcinogenesis by Bcl-2 in transgenic mice. *Cancer Res*. 1999;59(19):5017–5022.
17. Sansom OJ, et al. Myc deletion rescues Apc deficiency in the small intestine. *Nature*. 2007; 446(7136):676–679.
18. Cadoret A, et al. Hepatomegaly in transgenic mice expressing an oncogenic form of beta-catenin. *Cancer Res*. 2001;61(8):3245–3249.
19. Torre C, et al. The transforming growth factor-alpha and cyclin D1 genes are direct targets of beta-catenin signaling in hepatocyte proliferation. *J Hepatol*. 2011;55(1):86–95.
20. Bendelac A, Savage PB, Teyton L. The biology of NKT cells. *Annu Rev Immunol*. 2007;25:297–336.
21. Umeda T, Yamamoto T, Kajino K, Hino O. beta-catenin mutations are absent in hepatocellular carcinomas of SV40 T-antigen transgenic mice. *Int J Oncol*. 2000;16(6):1133–1136.
22. Crowe NY, et al. Differential antitumor immunity mediated by NKT cell subsets in vivo. *J Exp Med*. 2005;202(9):1279–1288.
23. Ovejero C, et al. Identification of the leukocyte cell-derived chemotaxin 2 as a direct target gene of beta-catenin in the liver. *Hepatology*. 2004;40(1):167–176.
24. Hiraki Y, et al. A novel growth-promoting factor derived from fetal bovine cartilage, chondromodulin II. Purification and amino acid sequence. *J Biol Chem*. 1996;271(37):22657–22662.
25. Mori Y, et al. Stimulation of osteoblast proliferation by the cartilage-derived growth promoting factors chondromodulin-I and -II. *FEBS Lett*. 1997;406(3):310–314.
26. Ong HT, Tan PK, Wang SM, Hian Low DT, Ooi LL, Hui KM. The tumor suppressor function of LECT2 in human hepatocellular carcinoma makes it a potential therapeutic target. *Cancer Gene Ther*. 2011;18(6):399–406.
27. Saito T, et al. Increase in hepatic NKT cells in leukocyte cell-derived chemotaxin 2-deficient mice contributes to severe concanavalin A-induced hepatitis. *J Immunol*. 2004;173(1):579–585.
28. Yamagoe S, Yamakawa Y, Matsuo Y, Minowada J, Mizuno S, Suzuki K. Purification and primary amino acid sequence of a novel neutrophil chemotactic factor LECT2. *Immunol Lett*. 1996;52(1):9–13.
29. Cui J, et al. Requirement for Valpha14 NKT cells in IL-12-mediated rejection of tumors. *Science*. 1997;278(5343):1623–1626.
30. Okumura A, et al. Suppressive role of leukocyte cell-derived chemotaxin 2 in mouse anti-type II collagen antibody-induced arthritis. *Arthritis Rheum*. 2008;58(2):413–421.
31. Kronenberg M, Gapin L. The unconventional lifestyle of NKT cells. *Nat Rev Immunol*. 2002;2(8):557–568.
32. Berzins SP, Smyth MJ, Baxter AG. Presumed guilty: natural killer T cell defects and human disease. *Nat Rev Immunol*. 2011;11(2):131–142.
33. Kim CH, Johnston B, Butcher EC. Trafficking machinery of NKT cells: shared and differential chemokine receptor expression among V alpha 24(+)V beta 11(+) NKT cell subsets with distinct cytokine-producing capacity. *Blood*. 2002;100(1):11–16.
34. Lee PT, Benlagha K, Teyton L, Bendelac A. Distinct functional lineages of human V(alpha)24 natural killer T cells. *J Exp Med*. 2002;195(5):637–641.
35. Tahir SM, et al. Loss of IFN-gamma production by invariant NK T cells in advanced cancer. *J Immunol*. 2001;167(7):4046–4050.
36. van der Vliet HJ, Wang R, Yue SC, Koon HB, Balk SP, Exley MA. Circulating myeloid dendritic cells of advanced cancer patients result in reduced activation and a biased cytokine profile in invariant NKT cells. *J Immunol*. 2008;180(11):7287–7293.
37. Schiechl G, et al. Tumor development in murine ulcerative colitis depends on MyD88 signaling of colonic F4/80+CD11b(high)Gr1(low) macrophages. *J Clin Invest*. 2011;121(5):1692–1708.
38. Huang F, Geng XP. Chemokines and hepatocellular carcinoma. *World J Gastroenterol*. 2010; 16(15):1832–1836.
39. Kim MY, et al. Tumor self-seeding by circulating cancer cells. *Cell*. 2009;139(7):1315–1326.
40. He G, Karin M. NF-kappaB and STAT3 - key players in liver inflammation and cancer. *Cell Res*. 2011; 21(1):159–168.
41. Rebouissou S, et al. Frequent in-frame somatic deletions activate gp130 in inflammatory hepatocellular tumours. *Nature*. 2009;457(7226):200–204.
42. Phesse TJ, et al. Deficiency of Mbd2 attenuates Wnt signaling. *Mol Cell Biol*. 2008;28(19):6094–6103.
43. Tannour-Louet M, Porteu A, Vaulont S, Kahn A, Vasseur-Cognet M. A tamoxifen-inducible chimeric Cre recombinase specifically effective in the fetal and adult mouse liver. *Hepatology*. 2002;35(5):1072–1081.
44. Jacque E, Tchenio T, Piton G, Romeo PH, Baud V. RelA repression of RelB activity induces selective gene activation downstream of TNF receptors. *Proc Natl Acad Sci U S A*. 2005;102(41):14635–14640.
45. Decaens T, et al. Stabilization of beta-catenin affects mouse embryonic liver growth and hepatoblast fate. *Hepatology*. 2008;47(1):247–258.
46. Miyagi T, et al. Concanavalin a injection activates intrahepatic innate immune cells to provoke an antitumor effect in murine liver. *Hepatology*. 2004; 40(5):1190–1196.